NTNU – Trondheim
Norwegian University of
Science and Technology

Effect of Non-spherical Voids on the Mechanical Behavior of Shape Memory Alloys

Tor Lone Rasmussen

Civil and Environmental Engineering
Submission date: June 2013
Supervisor: Zhiliang Zhang, KT

Norwegian University of Science and Technology
Department of Structural Engineering

Effect of Non-spherical Voids on the Mechanical Behavior of Shape Memory Alloys

Tor Lone Rasmussen

Spring 2013

Abstract

The use of shape memory alloys has seen a steady increase since its discovery. Understanding the mechanical behavior behind a ductile fracture of these materials is important to further the applicability of shape memory alloys. Some research on spherical microvoids in shape memory alloys has been conducted, but there is not much literature on non-spherical voids.

The effect of non-spherical microvoids on the mechanical behavior of shape memory alloys has been explored in this thesis. By running numerical simulations in the commercial finite element software Abaqus, several different void shapes and sizes were analyzed. The simulations were limited to uniaxial stress without superplasticity. The results suggest that the width of the void, not the heigth/width ratio or the void volume fraction, has the greatest influence on the transformation stresses. Due to the limitations of this thesis, further studies should be conducted.

The results had some differences compared to similar studies. The nature of the difference is unknown, and should be further explored. A more in-depth study with more shapes and void volume fractions is also needed to confirm the findings of this report. Both the effect of superplasticity, as well as a triaxial stress state may produce different results. A study of the effect of superplasticity should be emphasized, as plasticity is a very important part of a material's behavior.

Summary in Norwegian

Bruken av hukommelseslegeringer har hatt en gradvis økning etter at de ble oppdaget. For å kunne utvide deres bruksområder, er det viktig å forstå mekanikken bak duktile brudd i disse materialene. Effekten av sfæriske mikroporer har fått litt oppmerksomhet, men det er lite litterature om ikke-sfæriske porer.

I denne oppgaven er effekten av ikke-sfæriske porer på de mekaniske egenskapene til hukommelseslegeringer nærmere undersøkt. Numeriske simulasjoner er kjørt i Abaqus, hvor forskjellige poreformer og porestørrelser ble studert. Simulasjonene var begrenset til uniaksiell spenning uten superplastisitet. Resultatene antyder at porebredden, ikke høyde/bredde forholdet eller pore-volum forholdet, har størst påvirkning på transformasjons spenningene. På grunn av begrensningene i denne oppgaven burde mer dypt-gående analyser utføres.

Resultatene har også ulikheter med tilsvarende studier. Årsaken til disse ulikhetene er ukjente, men bør identifiseres. En dypere studie med flere pore-former og pore-volum forhold trengs også for å verifisere resultatene. En analyse med superplastisitet eller en triaksiell spenningstilstant bør også utføres for å danne et mer komplett bilde av materialets oppførsel. Særlig superplastisitet bør studeres, ettersom plastisitet er en naturlig del av materialets oppførsel.

Acknowledgments

I would like to thank my supervisor Zhiliang Zhang and co-supervisor Jim Stian Olsen for their contributions and support in writing this thesis.

Contents

List of Figures

List of Tables

1 Introduction

Shape memory alloys are a group of alloys capable of "remembering" its original state. It has two defining characteristics: the superelastic effect and the shape memory effect. In later years the material has seen an increased range of applications due to its high power density, solid state actuation, high damping capacity, durability and fatigue resistance [1].

Despite being discovered several years ago, little research has been done on shape memory alloys. Due to the increasing use of shape memory alloys, it is important to examine how a ductile fracture will affect the mechanical properties of the material.

This thesis will study the effect of non-spherical voids. It builds upon the work of Jim Stian Olsen and Zhiliang Zhang [2], where they examined the effect of spherical micro-voids in shape memory alloys.

Several models with different void shapes and sizes are modelled in Abaqus. By subjecting them to a uniaxial load, which is subsequently removed, produces the characteristic hysteresis.

Only superelasticity in a uniaxial stress state is tested. Some guidance for a triaxial stress test is supplied in chapter 3.2.

A basic look at the theory behind shape memory alloys and ductile fracture is presented in chapter 2, along with some continuum mechanics and a quick overview of the challenges in modeling ductile fracture.

In chapter 3 follows a description of how the models were modelled. The simulations are run in the commercial finite element software SIMULIA Abaqus FEA (Abaqus) and the results are processed in Microsoft Excel (Excel). It is assumed that the reader has basic knowledge of how Abaqus work, as only details that are somewhat unique for this type of problem are explained in detail.

The results are discussed in detail in chapter 4. The main points are divided into sub-chapters, with a unifying discussion in chapter 4.5. Conclusions and recommendations for further work are presented in chapter 5. The appendix contains input-data for Abaqus.

2 Theory

This thesis requires a basic understanding of shape memory alloys, ductile fracture and continuum mechanics. A brief overview of the relevant parts of these subjects is supplied in this chapter.

2.1 Shape memory alloys

Shape memory alloys are materials that are able to recover large strains, and capable of reverting to the original shape (thus the name shape memory). Shape memory alloys are known for the superelastic effect and the shape memory effect.

The superelastic effect allows the material to recover large strains without any permanent damage. This process will also absorb large amounts of energy, making it potentially useful for dampers and other energy absorbents. The shape memory effect allows the material to regain its original shape after deformation.

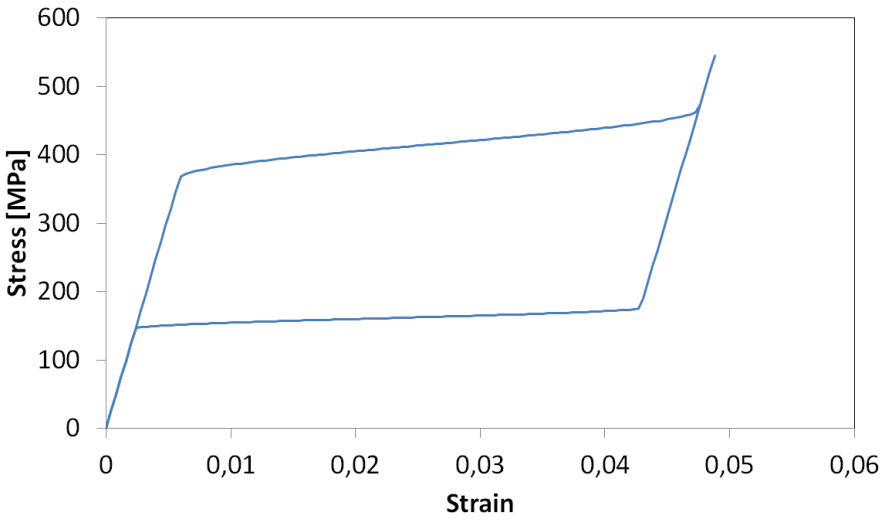

Figure 1: Superelasticity with the characteristic hysteresis.

Superelastic effect and the shape memory effect

These effects are governed by martensitic transformation. This is a diffusionless, or displacive, phase transformation in solids. The change in the atomic structure is a result of a cooperative movement of the atoms, not local diffusions. Martensitic transformation may only occur when both:

- The chemical free energy of the martensitic phase is lower than that of the original austenitic phase.
- The non-chemical free energy is smaller than the difference of chemical free energy between the two phases [2].

Superelasticity is mostly the result of non-thermoelastic transformation, which occurs when all non-chemical free energy (such as interface energy, elastic energy and energy needed to induce plastic deformation) are used. Contrary, the shape memory affect is mainly the result of thermoelastic transformation, where non-chemical free energy is negligible.

In the original phase, the austenitic phase, a material have a highly ordered body-centered cubic structure. When it is sufficiently cooled, phase transformation to martensite starts. To accommodate this change, the atoms starts twinning. Because of the low symmetry in the martensitic phase, several variations can form. This is called multi-variant (or temperature-induced) martensite.

As the material is deformed, the atoms starts detwinning. When the deformations are large enough, the atoms are forced into a single variant. This is called single-variant (or stress-induced) martensite. The deformation will remain when the stress is removed. This deformation differs from plastic deformations, as it is a result of a change of phase, not dislocation.

By heating the material, a phase transformation from stress-induced martensite to austenite is initiated. As the austenitic phase is highly symmetric, there is only one path for the reverse transformation. The material then regains the original shape.

The most common shape memory alloys are NiTi-based alloys, which are lightweight (due to the low density of titanium), easy to install and proven reliable [3]. There are alternatives to NiTi, such as Cu-based and Fe-based alloys. These are cheaper, but at the cost of quality.

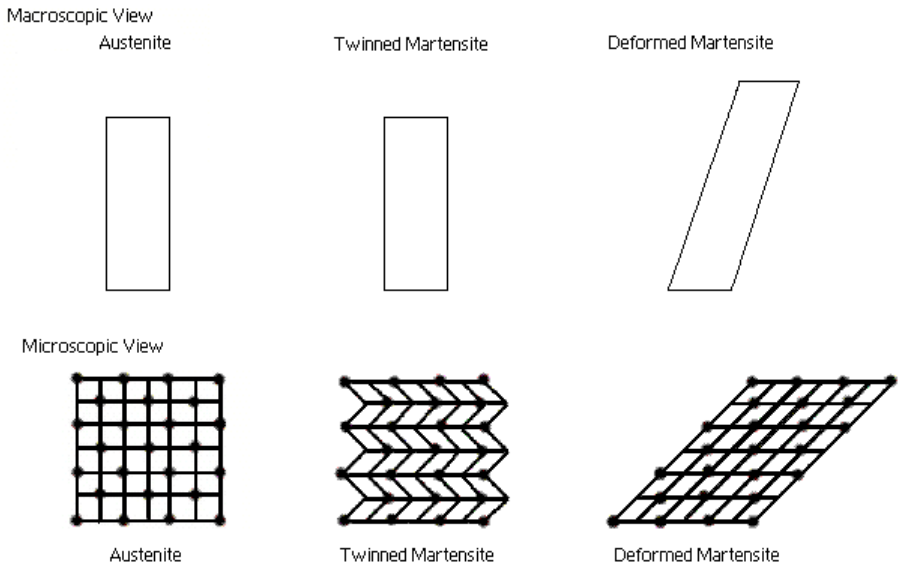

Figure 2: Different phases of the shape memory alloy.

Modeling of shape memory alloys

The amount of martensite in a material is defined as the martensitic fraction, ξ, which ranges from 0 to 1. Transformation between the phases starts and finishes at certain temperatures. The forward transformation from austenite to martensite starts at M_s and ends at M_f , while the reverse transformation starts at A_s and ends at A_f.

Due to the thermoelastic nature of shape memory alloys, there is an inverse relationship between stress and temperature. By increasing the stress in the material, the critical transformation temperatures are reduced. Thus phase transformation can be forced through applied stress.

The austenitic and martensitic phases of a shape memory alloy usually have different elastic modulus'. During transformation, the elastic modulus is modelled as a function of the martensitic fraction.

$$E = E(\xi) = E_A + \xi(E_M - E_A) \tag{2.1}$$

The austenitic phase is generally stiffer than the martensitic phase. An example of how the difference in elastic modulus can influence the stress-strain curve is illustrated in figure 3.

During transformation, a small increase in stress will produce large strains. This is

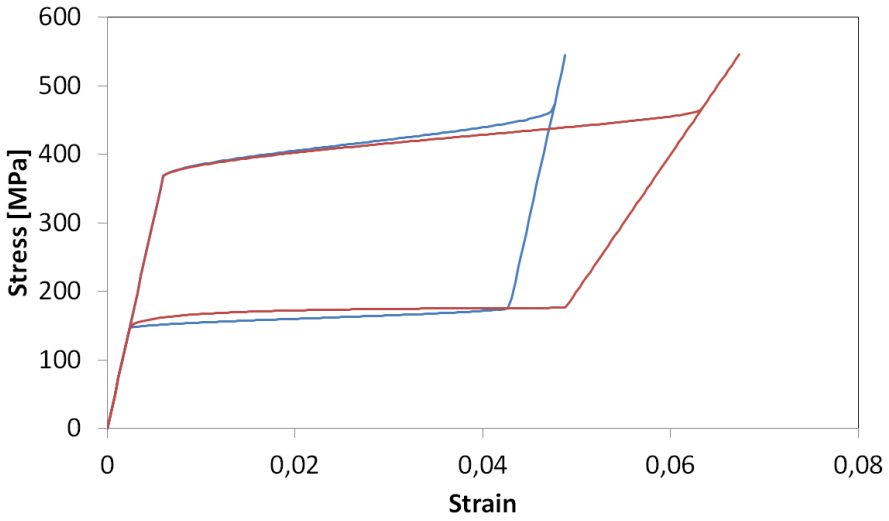

Figure 3: Comparison of different values of E_M. The red curve with $E_M = 1/3E_A$.

called the transformation plateau. If the material is loaded further after completing transformation, it will exhibit a normal elastic behavior until plastic yielding.

Plastic behavior stems from dislocations in the atom structure, which is different from the twinning and detwinnig effect. Plastic strains are non-recoverable. Because the start of transformation depends on temperature, care should be taken to ensure that the material does not yield to plasticity before transformation is commenced.

Although shape memory alloys are relatively durable, functional fatigue is an issue with prolonged use. Functional fatigue is a gradual diminishing of either the shape memory effect or the superelastic effect (depending on the materials application). The fatigue can be delayed by reducing the strain, or by using alloys with high melting temperature and mechanically strong austenite [4].

2.2 Ductile fracture

Ductile fracture occurs when a material fractures due to extensive plastic deformation. The process of ductile fracture has several stages.

When stress is applied to a material, a process called void nucleation is initiated. Second-phase particles, either added by design or unavoidable impurities, act as nucleation sites. Here the particles will break the local matrix material, either by debonding or cracking. This process is dependent on several factors, such as tem-

perature, particle size, shape, distribution, stress state and strength of the particle and interface [5]. Because of the complexity of this process, it is hard to create universal models. Different scenarios may require very different approaches in modeling. In general, there are two types of models for void nucleation: dislocation models and continuum models [6].

If the stress is maintained, the voids will grow. This is a continuum plastic deformation process. During this stage voids may change shape, depending on the stress state. As there is no internal pressure, the deformation of the voids is governed by the plastic flow of the material. This is a relatively stable stage of deformation. Voids will grow in the principal direction during uniaxial load. However, in a triaxial stress state the voids will grow laterally and flatten, independent of the principal strain direction [5].

The associated flow rule of martensitic and austenitic transformation, is assumed to be equivalent of the plastic flow due to yielding [7].

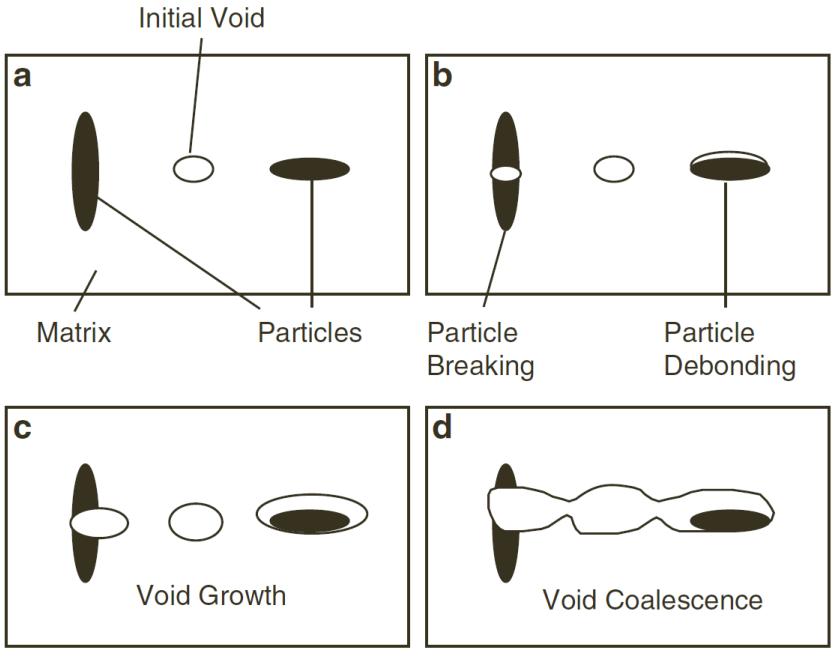

Figure 4: The different phases of ductile fracture [5].

The last stage is void coalescence. As long as stress is applied, the microvoids will continue to expand until they rapidly start linking up with other voids. The crack will propagate until failure.

Models describing the whole fracture process have been made. These are based

on two different approaches: A global approach, where the ductile fracture is regarded as a collective process controlled by global parameters. And a local approach, where the sub-processes leading to fracture are separated. Classical fracture mechanics has a global approach, while damage mechanics has a local approach [6].

An example of the latter type of model is the Gurson model [8]. It is based upon the upper bound theorem of plasticity. It states that a given kinematic admissible mechanism where the external work is set equal to the internal plastic work, will produce a capacity greater or equal to the real value [9].

The Gurson yield function, with additional parameters provided by Tvergaard [10], is presented for spherical voids in equation (2.2).

$$\Phi = \frac{\Sigma_{eq}^2}{\bar{\sigma}^2} + 2q_1 f \cosh\left(\frac{3q_2\Sigma_{hyd}}{2\bar{\sigma}}\right) - (1 + (q_1 f)^2) = 0 \tag{2.2}$$

Σ_{eq} = Conventional von Mises equivalent stress

$\bar{\sigma}$ = Flow stress of the matrix material

Σ_{hyd} = Hydrostatic stress

f = Void volume fraction

q_i = Tvergaard's Constants

Notice that a void volume fraction of 0 reduces the equation to the conventional Von Mises function for zero porosity.

To simulate the voids in a shape memory alloy, a unit-cell model is made. An axisymmetric model with a single void in the center can be regarded as an element in a doubly periodic array of regular hexagonal cylindrical cells. The hexagonal shape is approximated by the cylinder produced by the axisymmetric model [6].

A Gurson model modified for shape memory alloys have been suggested by Jim Stian Olsen [11]. He used the start of forward transformation stress as the matrix yield stress.

$$\Phi^{tr}(\Sigma,f,\xi) = \frac{\Sigma_{eq}^2}{\bar{\sigma}_f^{tr^2}} + 2q_1 f \cosh\left(\frac{3q_2\Sigma_{hyd}}{2\bar{\sigma}_f^{tr}}\right) - (1 + (q_1 f)^2) = 0 \tag{2.3}$$

Where $\sigma_f^{tr} = \sigma_f^{tr}(\xi)$ is the transformation flow stress.

2.3 Stress state

By calculating the stress and strain of the whole unit-cell model, the influence of the void size and shape on the material can be found. The local quantities within the unit-cell are denoted microscopic quantities and global quantities are called mesoscopic quantities.. The mesoscopic stress and strain tensors are denoted Σ_{ij} and E_{ij} respectively, while the microscopic stress and strain tensors are denoted σ_{ij} and ε_{ij}.

When analysing the model, the mesoscopic quantities are used. As the unit-cell model represents one element in a larger system, the mechanical behavior of the whole unit-cell is needed. Just like a tiny element in the Abaqus model only represents a part of a bigger model, the unit-cell is only a part of an even bigger system. This way the voids in a ductile material may be studied, without modeling more than one void.

Because of the axisymmetric model, there is no shear stress in the x- and y-direction. Thus the axial, radial and tangential directions are also the principal directions. Furthermore, due to symmetry, the radial and tangential stress and strain will be of equal magnitude.

The mesoscopic strain tensors are:

$$\begin{aligned} E_x &= ln\left(1 + \frac{u_x^a}{L_{x0}}\right) \\ E_y &= ln\left(1 + \frac{u_y^d}{L_{y0}}\right) \\ E_{eq} &= \frac{2}{3}|E_y - E_x| \end{aligned} \tag{2.4}$$

As the stress vector is constant along the edges of the model, the mesoscopic stresses are found as:

$$\begin{aligned} \Sigma_x &= \frac{F_y}{4\pi(L_{x0} + u_x^a)(L_{y0} + u_y^d)} \\ \Sigma_y &= \frac{F_x}{\pi(L_{x0} + u_x^a)^2} \end{aligned} \tag{2.5}$$

The mesoscopic hydrostatic and equivalent stresses are found as:

$$\begin{aligned} \Sigma_{hyd} &= \frac{\Sigma_y + 2\Sigma_x}{3} \\ \Sigma_{eq} &= |\Sigma_y - \Sigma_x| \end{aligned} \tag{2.6}$$

The stress triaxiality is defined in equation (2.7), where ρ is the stress proportionality factor. $\rho = 0$ ($T = 1/3$) represents a uniaxial stress state.

$$T = \frac{\Sigma_{hyd}}{\Sigma_{eq}} = \frac{1}{3}\left(\frac{1+2\rho}{|1-\rho|}\right) \tag{2.7}$$

$$\rho = \frac{\Sigma_x}{\Sigma_y} = \frac{3T-1}{3T+2} \tag{2.8}$$

Where ρ is the loading parameter.

From equation (2.7) and equation (2.2) it can be seen that the intensity of the hydrostatic stress depends on the stress triaxiality. Thus it is important to achieve a constant stress triaxiality during the simulation. This will be further explored in section 3.2.

3 Method

3.1 Overview

The main purpose of this thesis is to study the effect of non-spherical voids on the mechanical properties of shape memory alloys. This is achieved by comparing the stress-strain plots and the start of transformation stresses of models with different microvoid shapes and sizes.

The voids are modelled as ellipsoidals, while the hexagonal cells are approximated as cylinders, thus enabling the use of axisymmetric models [10]. Two parameters define non-spherical voids, the aspect ratio a and the void fracture f. To ensure a wide range of data to analyse, several models with varying aspect ratios and void fractions are made.

$$a = \frac{r_h}{r_w} \tag{3.1}$$

$$f = \frac{2r_h r_w^2}{3L_{x0}^2 L_{z0}} \tag{3.2}$$

The models are made with void fractions of $f = 0{,}001$, $f = 0{,}010$ and $f = 0{,}050$, and aspect ratios ranging from $a = 0{,}25$ to $a = 4{,}00$. A model with $a = 4{,}00$ and $f = 0{,}050$ is not made because the height of the void exceeded the height of the model.

Due to software problems, only uniaxial tests have been run. A theoretical implementation of a triaxial stress state is given in this chapter.

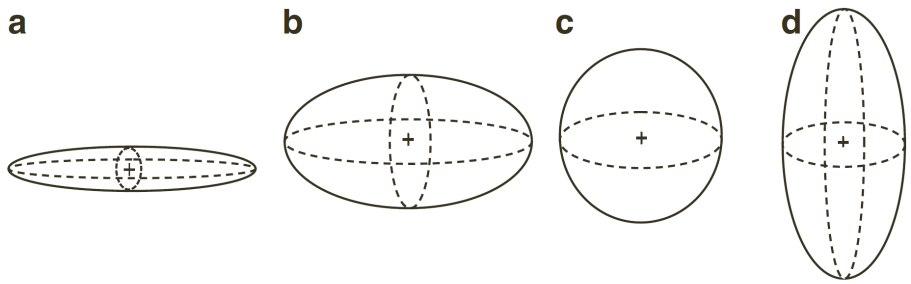

Figure 5: Example of different void shapes: a) Penny-shaped b) Oblate c) Sphere d) Prolate [5].

3.2 Modeling of test specimen in Abaqus

Creating an axisymmetric model is straightforward in Abaqus. In such a model the y-axis is the axis of revolution, while the x-axis is the radial direction. Thus only a cross section of the X-Y plane, with x ranging from $x = 0$ to $x = L_{x0}$ is needed. To reduce computational time, the model is cut in half at $y = 0$ and appropriate boundary conditions are added. The edge $x = 0$ is prevented from moving in the radial direction and the edge $y = 0$ is prevented from moving in the axial direction. The dimensions are shown in figure 6.

All models have a height of L_{y0} and a radius of L_{x0}. Thus simulating a cylinder with a height of $H = 2L_{y0}$ and a radius of $R = L_{x0}$, with a void in the center. As this is a unit-cell, the units of the dimensions are not important.

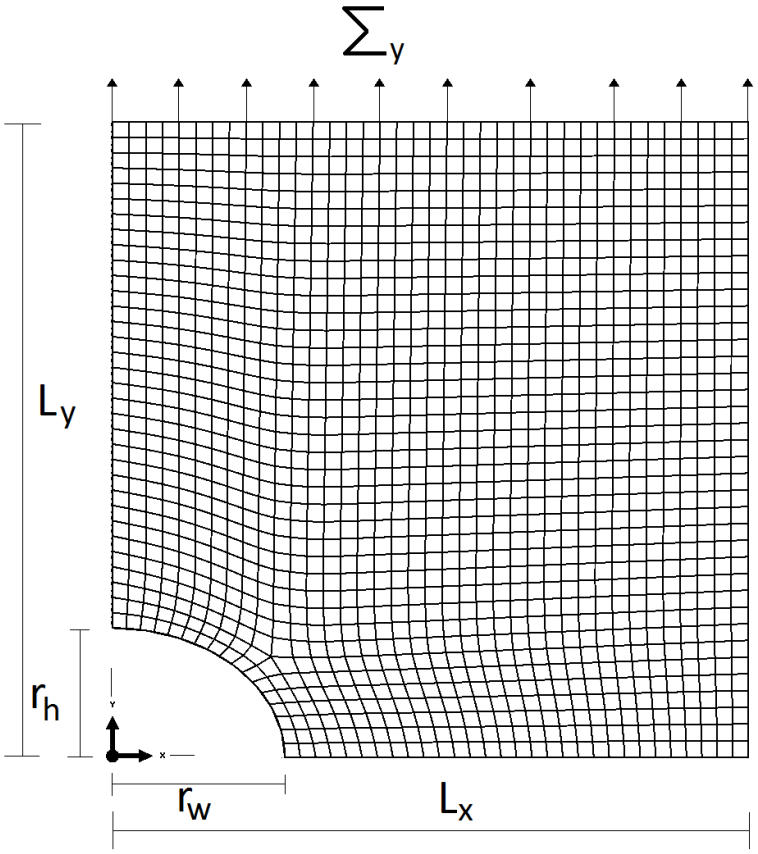

Figure 6: Example of axisymmetric model.

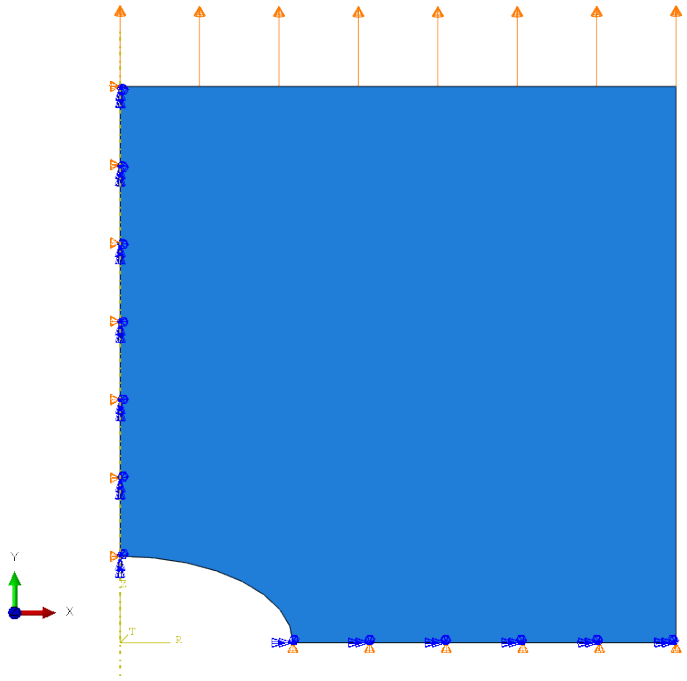

Figure 7: Boundary conditions and displacement of model with $a = 0{,}50$ and $f = 0{,}010$.

The strains in this model are expected to exceed $\varepsilon = 0{,}01$, thus small strains simplifications may not be used [9]. Non-linear geometry is thus enabled during the simulations.

Achieving convergence may be an obstacle due to the highly non-linear nature of the problem, but careful adjustment of increment sizes will provide satisfactory results.

To prevent the model from exploding due to a poorly calibrated load, a forced displacement is applied. It is placed along the top edge ($y = L_{y0}$) in the loading step, and then subsequently removed in the unloading step.

With an axisymmetric model, the reaction force of each node is the sum of the nodal force circumnavigating the figure, thus the sum of all the nodal axial reaction forces is the total axial reaction force [12].

The mesh is structured and made of 8-node biquadratic elements with reduced integration (called CAX8R in Abaqus), which is sufficient for this type of problem [2]. Each model contains approximately 1500 elements.

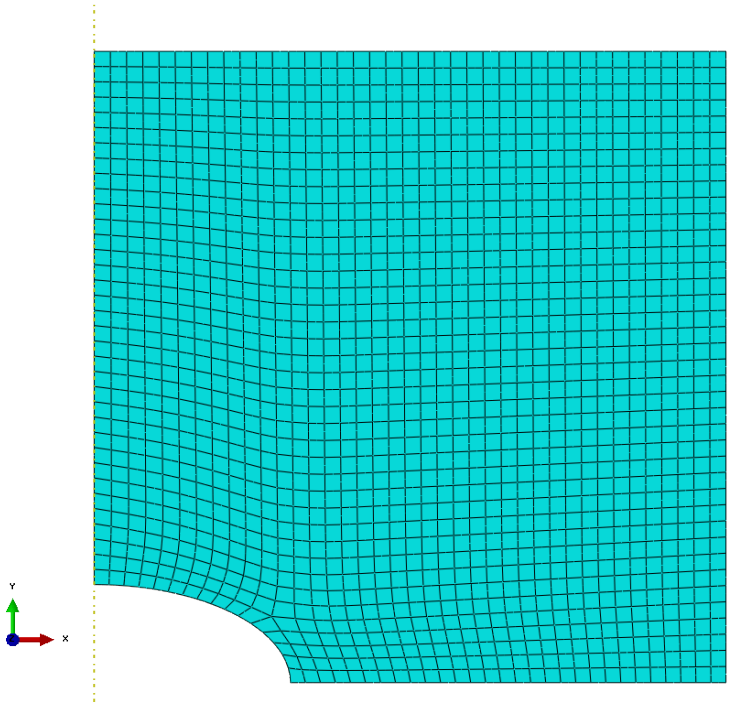

Figure 8: The mesh of the model in figure 7.

UMAT

Shape memory alloys requires material parameters that may not be entered into Abaqus through the standard input method. Abaqus is bundled with several user subroutines that are created to help users with problems that are not fully implemented in the software. One such subroutine is the User Material subroutine (UMAT in Abaqus/Standard). By entering the material parameters according to instructions provided by Simulia [13], Abaqus can simulate the superelastic effect (and superelastic-plastic).

Abaqus employs the algorithms by Auricchio and Taylor [14]. UMAT subroutines are not usable with other material parameters, thus the Gurson model can currently not be combined with shape memory alloys. The input used in this thesis is supplied in Appendix A, while the material data is presented in table 1.

Parameter	*Value*	*Description*
E_A	62000 MPa	Austenite elasticity
ν_A	0,33	Austenite Poisson's Ratio
E_M	62000 MPa	Martensite elasticity
ν_M	0,33	Martensite Poisson's Ratio
ε^L	0,04	Transformation strain
$\left(\frac{\delta\sigma}{\delta T}\right)_L$	6,7 MPa/°C	$\delta\sigma/\delta T$ loading
σ_L^S	440 MPa	Start of transformation loading
σ_L^E	540 MPa	End of transformation loading
T_0	11 °C	Reference temperature
$\left(\frac{\delta\sigma}{\delta T}\right)_U$	6,7 MPa/°C	$\delta\sigma/\delta T$ unloading
σ_U^S	250 MPa	Start of transformation unloading
σ_U^E	220 MPa	End of transformation unloading
σ_{CL}^S	0	Start of transformation stress during loading in compression, as a positive value
ε_V^L	0,04	Volumetric transformation strain
N_A	0	Number of annealings to be performed during the analysis

Table 1: Material data.

Multi-Point Constraints

Triaxiality is dependent on the ratio of Σ_x and Σ_y, which again depends on the volume of the model. Because this volume is constantly changing due to the applied deformation, it is hard to predict the volume after the deformation. Thus, achieving constant triaxiality cannot be done by applying a radial deformation.

A system was created by Søvik to counteract this problem [6]. A set of springs are added to the bottom right corner node, k_1, and to the top left corner node, k_2. As $F = uk$. Equations (2.5) are then rewritten:

$$\Sigma_y = \frac{(u_y^d - u_y^c)k_y}{\pi(L_{x0} + u_x^b)^2} \tag{3.3}$$

$$\Sigma_x = \frac{(u_x^a - u_x^b)k_x}{4\pi(L_{y0} + u_y^c)(L_{x0} + u_x^b)} \tag{3.4}$$

Combining them gives the following relation:

$$u_x^a = u_x^b + 2\rho\frac{k_y}{k_x}\frac{(u_y^d - u_y^c)(L_{y0} + u_y^c)}{L_{x0} + u_x^b} \tag{3.5}$$

By constraining the edge $x = L_{x0}$ to u_x^a, the model will be in a constant state of the given triaxiality. By setting $\rho = 0$, $T = 0.33$ a uniaxial stress state is achieved.

This can be implemented in Abaqus by use of the Multi-Point Constraint (MPC) subroutine. The node u_x^a is forced laterally according to equation (3.5), through the MPC subroutine. The rest of the nodes along the edge $x = L_{x0}$ may then be constrained to follow u_x^a with use of the *Equation function. A suggestion for a subroutine is supplied in Appendix A. Note that Abaqus requires an approved Fortran compiler to run this subroutine.

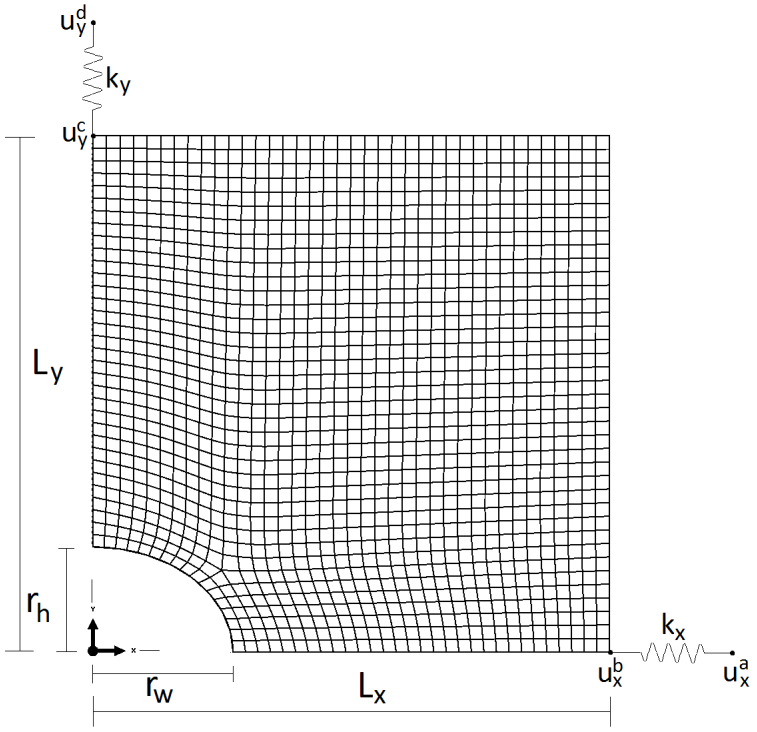

Figure 9: Søvik's spring model.

4 Results

4.1 Overview

Several different combinations of void volume fractions and aspect ratios have been considered.

4.2 Effect of void aspect ratio

As seen in figure 10 and 11, there is not much difference between void volume fractions as low as $f = 0{,}001$ and $f = 0{,}010$. The void shape seems to be irrelevant for void volume fractions of 1% and lower.

The results in figure 10 are indistinguishable from an analysis with no void (not shown here). In figure 11 there is a slight decrease in the start of forward transformation as the void shape flattens, with $a = 0{,}25$ being noticeably lower than others.

Figure 12 shows a significant reduction in the start of forward transformation stress for $a = 0{,}25$. There seems to be a pattern of a decreasing start of forward transformation along with a decreasing aspect ratio. However, even at a void volume fraction of $f = 0{,}050$, there is not much difference between sphere shaped voids and prolate shaped voids ($a \geq 1{,}00$).

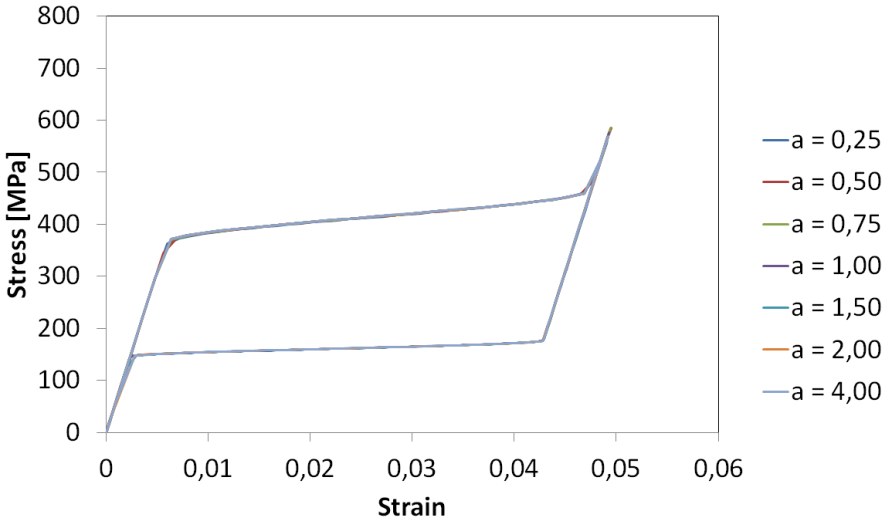

Figure 10: Stress-strain curve with $f = 0{,}001$.

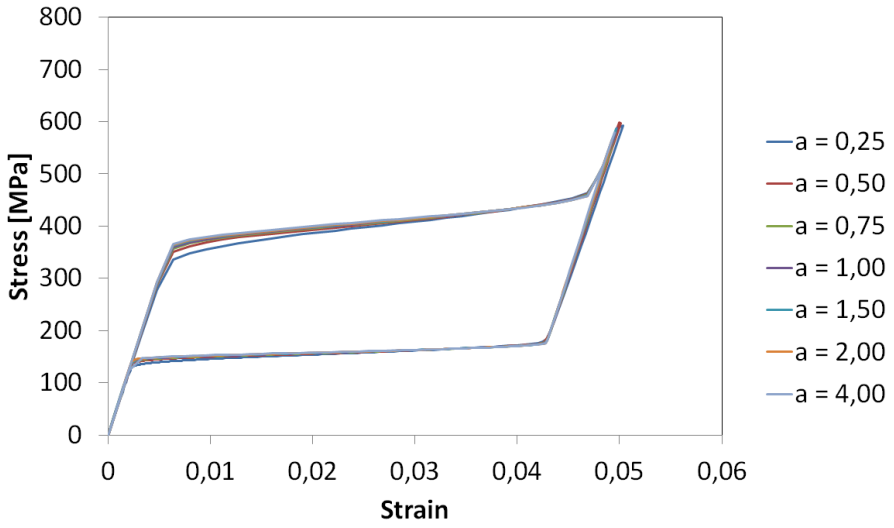

Figure 11: Stress-strain curve with $f = 0{,}010$.

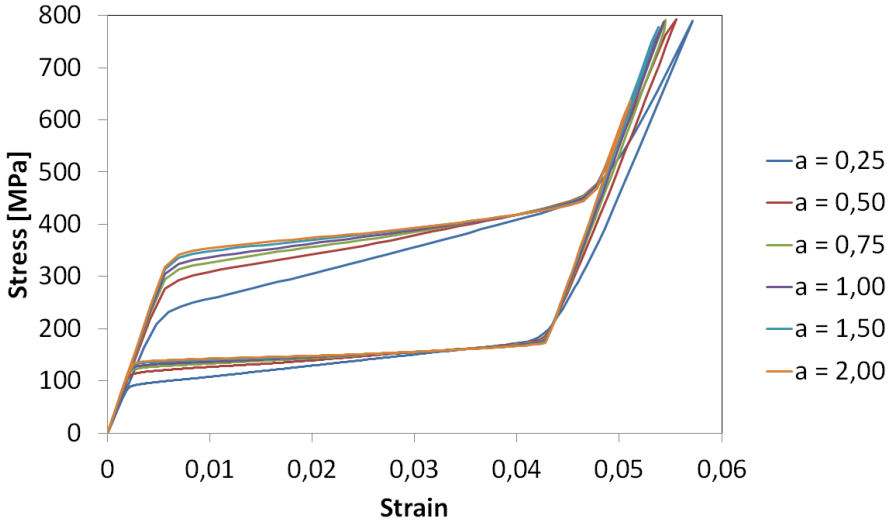

Figure 12: Stress-strain curve with $f = 0{,}050$.

Figure 12 also differs from the others in the elastic parts of the curves. With a low aspect ratio the elastic slopes are more gradual than the higher aspect ratios, despite all the curves having exactly the same elastic modulus both in the austenitic and martensitic phases.

This reason might be because different part of the unit-cell completes transformation at different times. These patterns are clear with penny-shaped voids, while

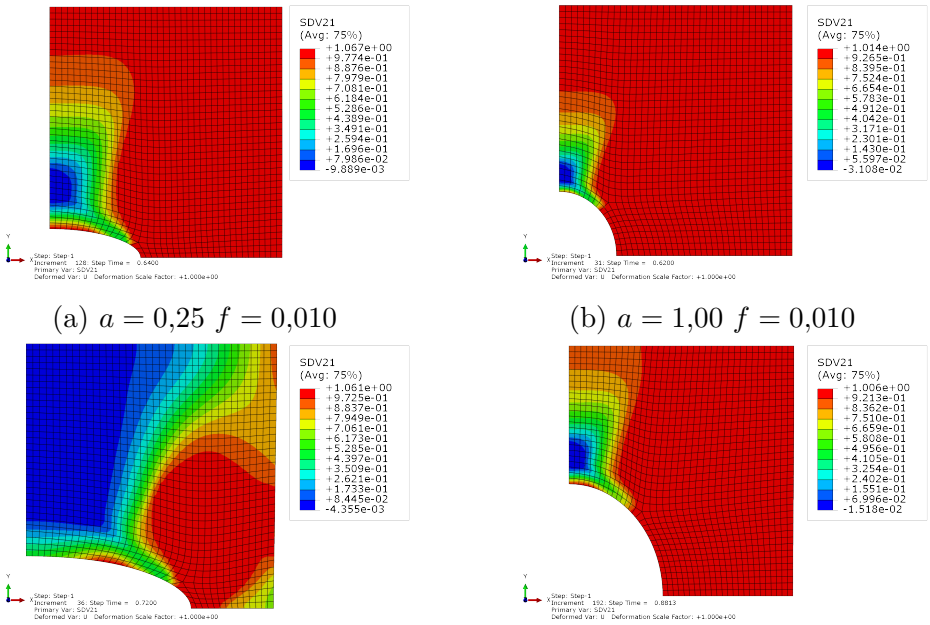

(a) $a = 0{,}25$ $f = 0{,}010$ (b) $a = 1{,}00$ $f = 0{,}010$

(c) $a = 0{,}25$ $f = 0{,}050$ (d) $a = 1{,}00$ $f = 0{,}050$

Figure 13: The martensitic fraction in the different models with a mesoscopic stress of approximately 600 MPa. Red indicates a martensitic fraction of $\xi = 1$ and blue is $\xi = 0$.

being more diminutive as a increases. There are also signs of a delay of the end of forward transformation.

The martensitic fraction

A comparison of the martensitic fractions with a mesoscopic stress of approximately 600 MPa can be seen for four models in figure 13. The martensitic fraction follows a pattern in three of the four figures. By comparing these figures to the curves in figures 11 and 12, a correlation between the decrease of start of transformation stress and lack of martensitic transformation can be seen.

A comparison of the martensitic fraction and stress field of two models is shown in figure 14 and 15. The martensitic fraction corresponds the the stress field of the unit-cell. The uneven stress distribution in figure 14b leads to the difference in martensitic transformation seen in figures 14a and 13c (figures 14a and 13c were made at a different time increments).

The stress in figure 14b does not envelop the void, but travels straight upwards

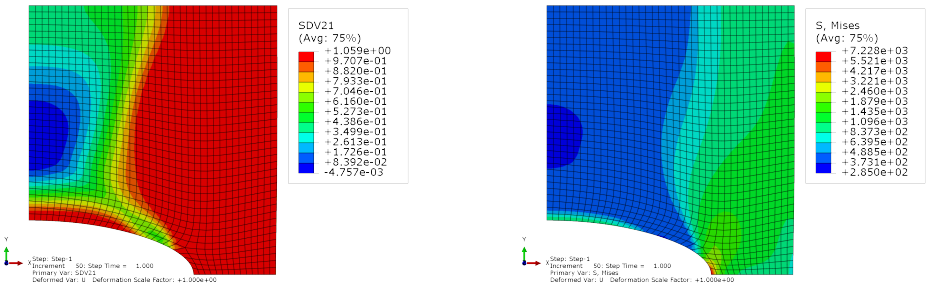

(a) Martensitic fraction ξ. (b) Von Mises stress.

Figure 14: Comparison of the martensitic fraction and the stress field of model with $a = 0{,}25$ and $f = 0{,}050$.

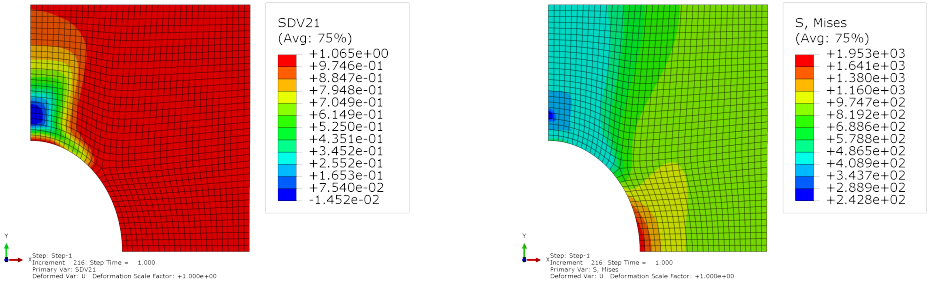

(a) Martensitic fraction ξ. (b) Von Mises stress.

Figure 15: Comparison of the martensitic fraction and the stress field of model with $a = 1{,}00$ and $f = 0{,}050$.

in the principal stress direction. Contrary, the stress in figure 15b is more evenly distributed. The decrease in the start of transformation stress seems to be a consequence of an uneven stress distribution in the unit-cell.

Plasticity

All the tests are run without plasticity, which may give inaccurate answers. As the void-width of $a = 0{,}25$ with $f = 0{,}050$ is $2/3L_{x0}$ there is a considerable elastic deformation in the void walls. This part of the unit-cell will finish transformation much faster than other parts, thus increasing both the overall stress and strain of the model, which might be another reason for the curves shown in figure 12.

The stress field of a model with $a = 0{,}25$ and $f = 0{,}050$ is shown in figure 16. The lack of plasticity means the stiffness of the elements is overestimated in some areas. Instead the elements will continue to resist deformation during the simulations. In reality, these critical zones would reach the yield stress and plastic flow would occur.

The exact yield stress of the material used in this report is unknown. Yield strength is highly dependent on temperature and alloy composition [15] and can range from 500 MPa to above 1400 MPa. The figure shows a considerable stress field across the unit-cell wall, with extremely high stress in the void corner.

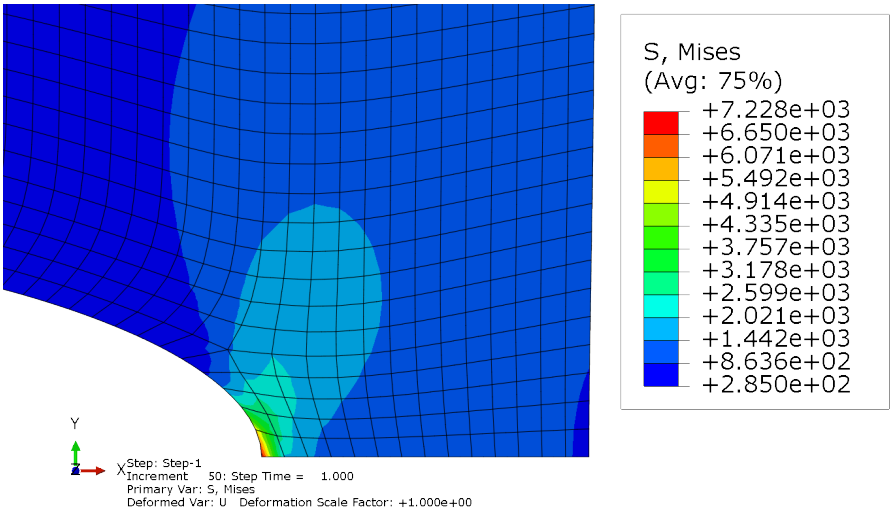

Figure 16: Stress field of model with $a = 0{,}25$ and $f = 0{,}050$.

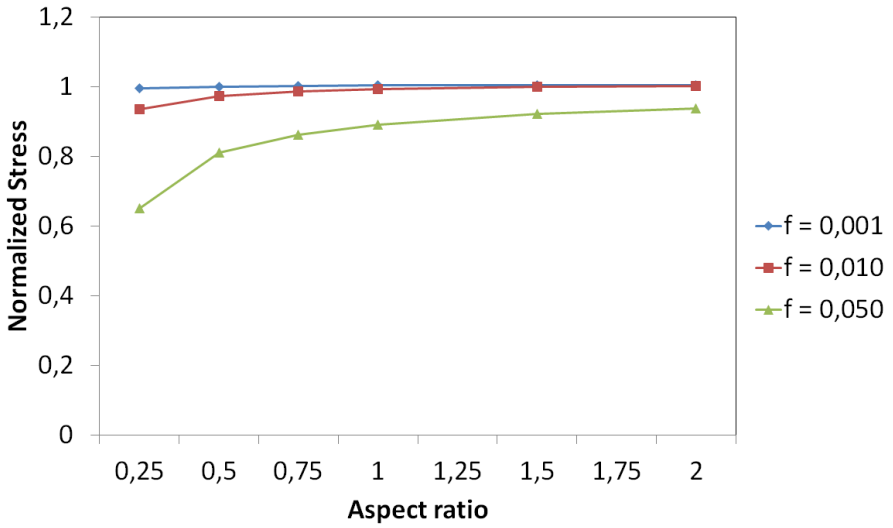

Figure 17: Start of forward transformation.

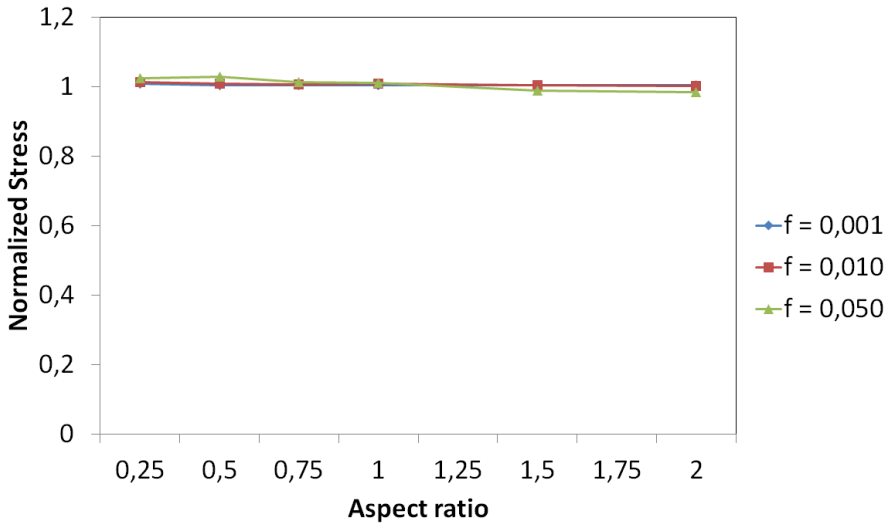

Figure 18: Start of backward transformation.

Start of transformation stresses

The differences in the start of transformation stresses is shown in figures 17 and 18. While there are large differences in the start of transformation stresses, there are no discernable differences in the start of backward transformation stresses.

The stress at the start of transformation from austenite to martensite is here found

as the stress in the first increment when $\mu < 1$, where μ is defined as

$$\mu = 10^{-4}\frac{\Delta\Sigma}{\Delta t} \tag{4.1}$$

The same criteria is used to find the start of transformation from martensite back to austenite. The start of forward and backward transformation stress are presented in figures 17 and 18.

There is a distinct reduction of the start of forward transformation stress for the model with $a = 0{,}25$ and $f = 0{,}050$, as dicussed earlier. If aspect ratios of $a = 0{,}50$ and lower are excluded, the start of transformation stresses seem to vary little with increasing aspect ratios. While $f = 0{,}001$ and $f = 0{,}010$ only show negligible differences, there is an overall clear reduction for $f = 0{,}050$.

At some point the void volume fraction seems to produce and overall reduction in the start of transformation stresses. However for oblate and penny-shaped voids, the aspect ratio seems to have more of an influence, likely due to the change in the stress field, as discussed earlier.

What is curious in all these figures is the lack of change in the start of backward transformation stress. Even the most extreme case of $a = 0{,}25$ with $f = 0{,}050$ shows no noticeable change in this stress.

4.3 Effect of void volume fraction

A rearrangement of the plots is shown in figure 19. These further illustrates the remarks in section 4.2. In forward transformation, the aspect ratio appears to be the dominant parameter for oblate shaped voids, while the void volume fraction plays a bigger role in more prolate shapes.

Notice how the reduced aspect ratio only seem to change the start of transformation stresses, while the increase in void volume fraction produces a downward shift of the entire upper part of the hysteresis.

As noted in the previous section, the start of the backward transformation remains unchanged for all aspect ratios and all void volume fractions. This not only contradicts the tendency of reduced transformation stress with a reduction of a and increase of f, it also contradicts the results of other reports [11]. J. S. Olsen found a downward shift of the entire hysteresis as the void volume fraction increased. He only studied spherical voids, thus the model shown in figure 20 should show the

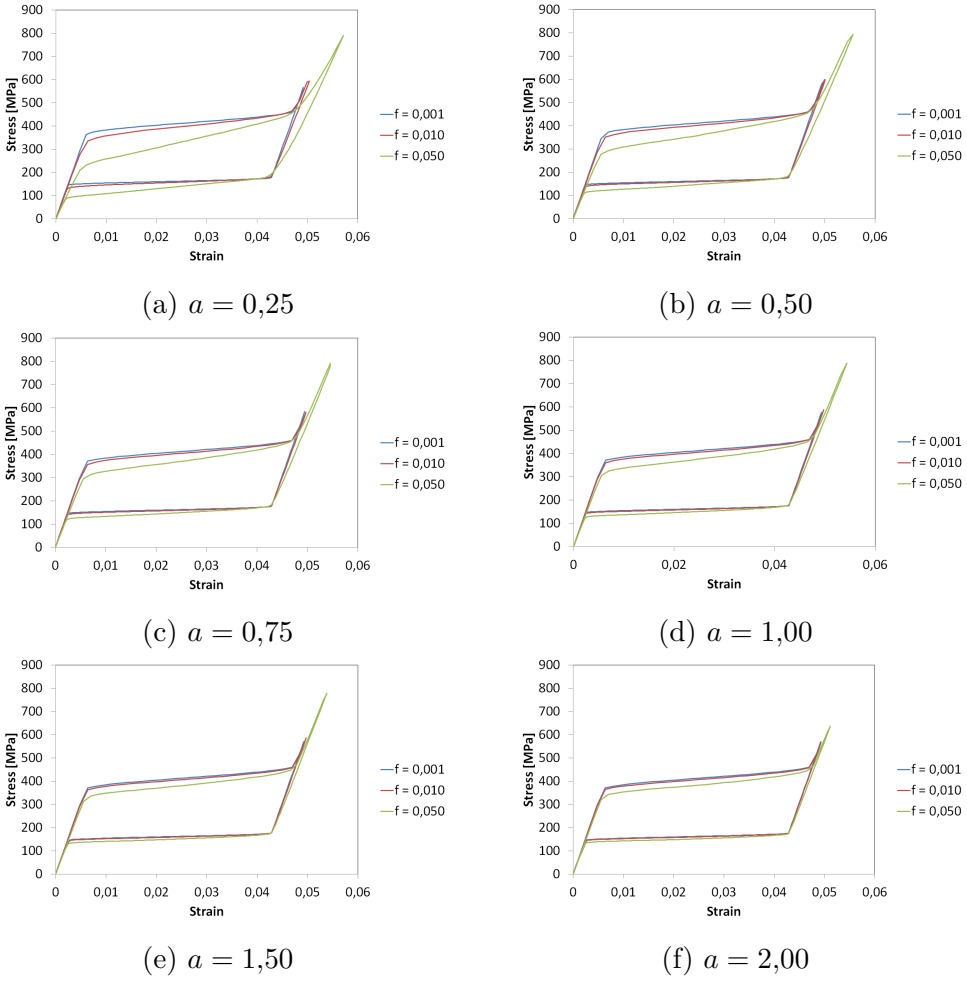

(a) $a = 0{,}25$ (b) $a = 0{,}50$

(c) $a = 0{,}75$ (d) $a = 1{,}00$

(e) $a = 1{,}50$ (f) $a = 2{,}00$

Figure 19: Different void shapes.

same downward shift. There is a downward shift on the left side of the hysteresis, but no equivalent shift on the right side, as Olsen found.

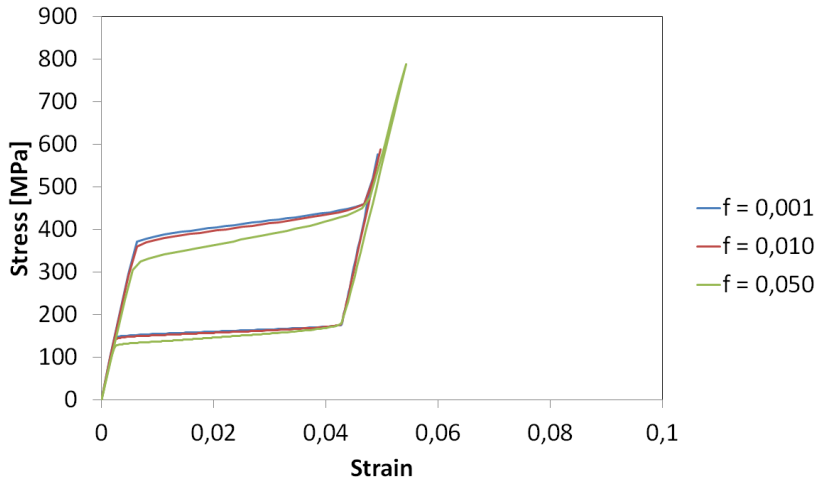

Figure 20: Stress-strain diagram for spherical voids with $E_M = E_A$.

Even though Olsen used another material in the tests, the only notable difference was a reduction in the elastic modulus in the martensitic phase. An analysis with $E_M = 1/3E_A$ is shown in figure 21.

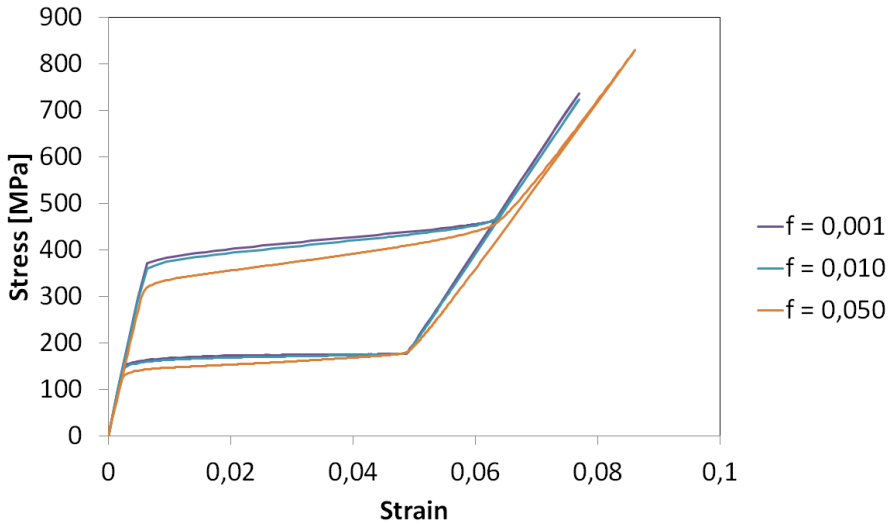

Figure 21: Stress-strain diagram for spherical voids with $E_M = 1/3E_A$.

Although there is more of a downward shift, especially at the left side of the hysteresis, the start of backward transformation clearly remains fixed on the same

stress for all void volume fractions. The elastic phase of the martensite for $f = 0{,}050$ is more gradual than in figure 20, though this is most likely due to the same mechanics discussed in section 4.2, exaggerated because of the reduction in E_M.

The reason for the discrepancies between the models is unknown. It is suggested in Olsen's paper that he used superplasticity in all models. The lack of plasticity may be the reason.

4.4 Effect of void width

To further test the influence of void shapes, models with a constant width are made. These models have the same aspect ratios used earlier, with the corresponding void volume fracture shown.

These figures show that the start of the forward transformation stress is barely affected by the increasing height, and thus void volume fraction, of the void. As seen in figure 25, an increase in the void width reduces the start of transformation, but any further change to the void shape has a very limited effect.

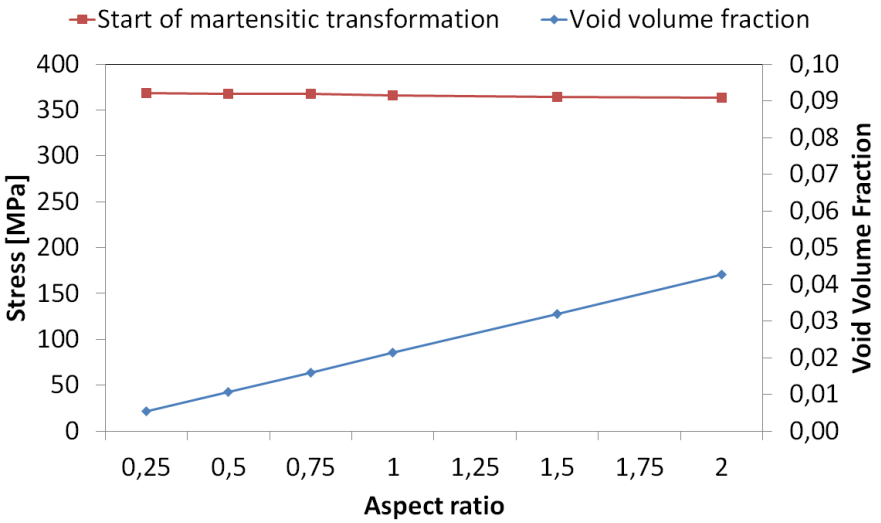

Figure 22: Start of martensitic transformation with $r_w = 0{,}2L_{x0}$.

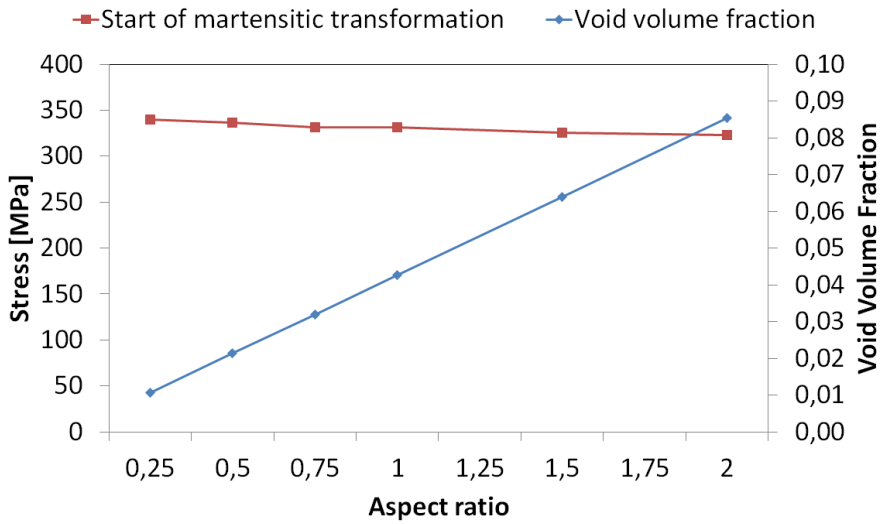

Figure 23: Start of martensitic transformation with $r_w = 0{,}4L_{x0}$.

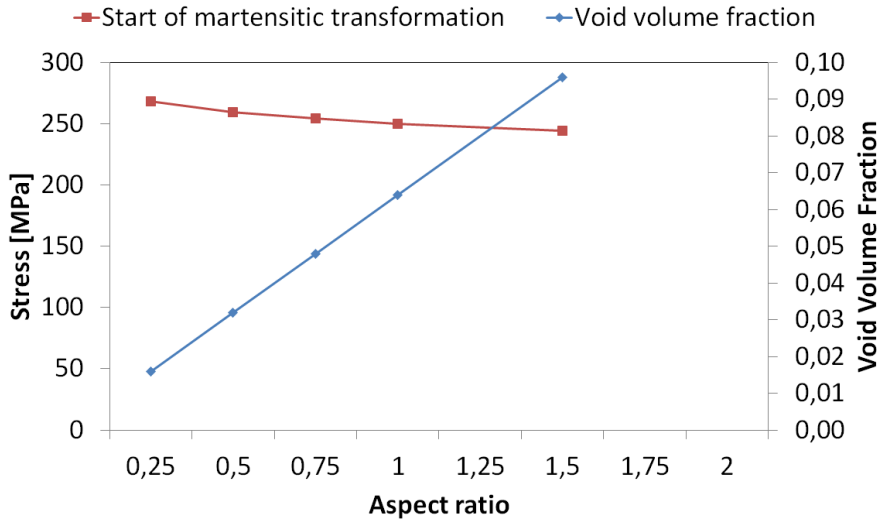

Figure 24: Start of martensitic transformation with $r_w = 0{,}6L_{x0}$. A model with $a = 2$ is not shown as the heigth of the void exceeds the heigth of the model.

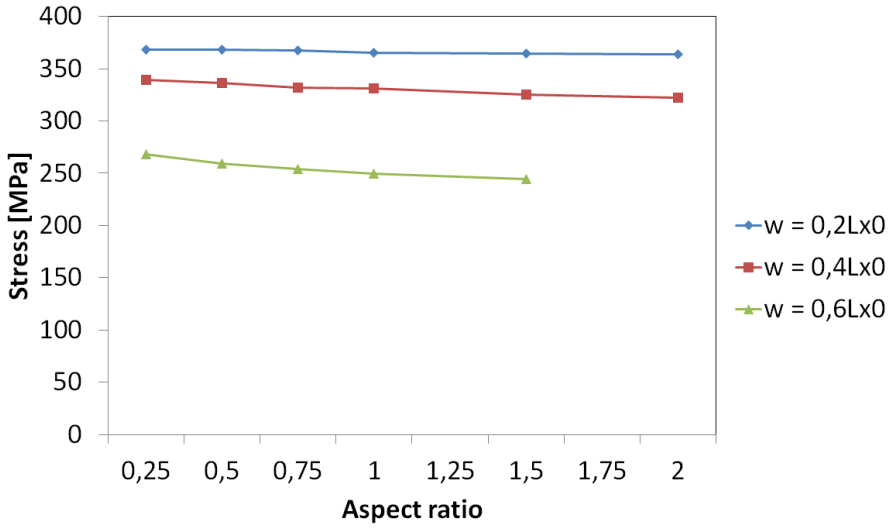

Figure 25: Effect of void width.

The increasing void volume fraction does not decrease the start of transformation stresses notably. Thus it seems the void volume fraction is less important than what was expected from the results in section 4.2.

From these figures it seems that only the width of the void, independent of void volume fraction and aspect ratio, affects the start of the forward transformation stress.

4.5 Discussions

Void width

The most noteworthy result of the simulations is the importance of the void width. It is interesting that the void shape and void volume fraction have comparatively little influence on the mechanical behavior of the material, despite their general importance in ductile fracture.

Voids will grow in the principal direction during uniaxial load. This means a penny-shaped void could expand into a prolate void, thus increasing the void volume fraction considerably, without notably affecting the start of transformation stress. A material in a uniaxial stress state may be subjected to considerable strain before the critical stress is reduced.

In a triaxial stress state the void will expand laterally and flatten, independent of the principal stresses [5]. This will increase the woid vidth as stress is applied. However, it is unknown whether the void width has the same influence on the material in a triaxial stress state.

Figure 17 in section 4.2 shows an overall reduction in the start of transformation stress for $f = 0{,}050$, compared to the similar stresses of $f = 0{,}001$ and $f = 0{,}010$. While the latter is ten times the size of the smallest void, and only a fifth of the largest void, only the largest void has a notable difference in start of transformation stress. This suggests a non-linear relationship between the void volume fraction (and thus void width) and the start of transformation stress.

Figure 26 compares the start of forward transformation stress with the area of the cross-section of the void in the xz-plane. It suggests a linear relationship between the area of the void perpendicular to the uniaxial stress direction and the start of transformation stress. Thus the start of transformation stress may have a quadratic relationship with the void widt. However, this result is highly uncertain due to the lack of data points.

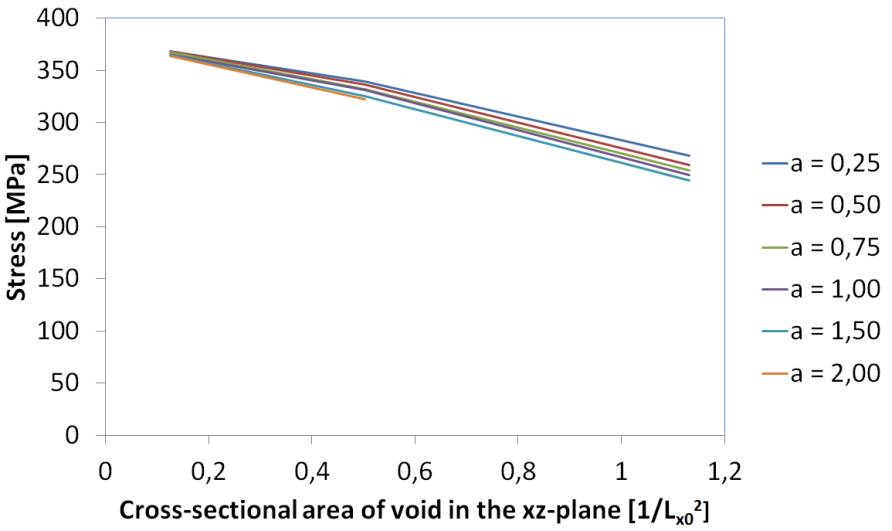

Figure 26: The start of forward transformation stress compared to the area of void cross-section.

Stress distribution

Section 4.2 suggests the reduction of the start of transformation stress stems from a change in the stress field pattern. The transition from the relatively even stress distribution seen in figure 15b, to the pillar-shaped distriuion in figure 14b is uncertain. As the start of transformation stress may be critically reduced beyond a certain void width, it is important to know at what threshold the stress field will change.

In a triaxial stress state, the stress field will most likely behave differently. If the impact of the void width is due to the distribution of the stress field, the void width will probably not be as important in a triaxial stress state, though this might depend on the triaxiality T.

This further suggests that it is the distribution of the stress field that influences the start of transformation stress, while the void width influence this stress field.

5 Conclusions and Further Work

Conclusions

These models have produced interesting results. There are strong indications that the start of transformation stress is governed by the stress distribution in the unit-cell, which seems to be controlled by the void width.

The simulations are all run in a uniaxial stress state. As the stress will be more evenly distributed in triaxial stress state, there is reason to believe that the void width in itself will be less important in non-uniaxial stress states.

There are some uncertainties in these results, such as the small range of void volume fractions modelled and lack of a deeper study of the stress fields. The lack of consistency with Olsen's results are also noteworthy. As the reason for this discrepancy is unknown, it might invalidate the results of this thesis.

Further work

This report has produced a very basic set of results, with many opportunities for further study. Models with a wider range of void volume fractions and void widths should be made to substantiate the results in this report.

An effort to reproduce these results would be very beneficial, as they might give a better understanding of both the mechanics of the change of transformation stress, but also help enlighten why these results differ from Olsen's.

The effect of plasticity has only been mentioned briefly in this report. All the simulations should be run with superplasticity as well. This may produce very different results and could also explain the difference from Olsen's paper.

As of now, the only way to model superelasticity in Abaqus is through the user material subroutine, which cannot be combined with Gurson. By rewriting the shape memory alloy subroutine to account for the modified Gurson, as proposed by Olsen (equation (2.3)), the effect of spherical voids can be further studied. This will require a good understanding of both the programming language Fortran as well as the user subroutine algorithms employed by Abaqus.

The relationship between the void shape (and particularly the void width) and the stress field should be further explored. By running the models in a triaxial stress state, with varying triaxialities, a more complete picture may be produced.

References

[1] H.-N. Li G. Song, N. Ma. Applications of shape memory alloys in civil structures. *Engineering Structures*, 28(9):1266–1274, July 2006.

[2] Jim Stian Olsen. *Constitutive behavior and fracture of shape memory alloys*. PhD thesis, Norwegian University of Science and Technology, 2012.

[3] C. M. Wayman K. Otsuka. *Shape Memory Materials*. Cambridge University Press, 1998.

[4] E. Hornbogen. Review thermo-mechanical fatigue of shape memory alloys. *Journal of Materials Science*, 39(2):385–399, 2004.

[5] C. Butcher Z. Chen. *Micromechanics Modelling of Ductile Fracture*. Springer, 2013.

[6] Odd Perry Søvik. *Numerical Modelling of Ductile Fracture - A Damage Mechanics Approach*. PhD thesis, Norwegian University of Science and Technology, 1996.

[7] Yuan-Yao Qian F. Trochu. Nonlinear finite element simulation of superelastic shape memory alloy parts. *Computers & Structures*, 62(5):799–810, 1997.

[8] A.L. Gurson. Continuum theory of ductile rupture by void nucleation and growth. part i. yield criteria and flow rules for porous ductile media. *Journal of Engineering Materials and Technology*, 99(2), 1977.

[9] Fridtjov Irgens. *Continuum Mechanics*. Springer, 2008.

[10] V. Tvergaard. On localization in ductile materials containing spherical voids. *International Journal of Fracture*, 18(4), 1982.

[11] Z. L. Zhang J. S. Olsen. Effect of spherical micro-voids in shape memory alloys subjected to uniaxial loading. *International Journal of Solids and Structures*, 49(14):1947–1960, July 2012.

[12] SIMULIA. *Abaqus User's Manual Ver. 6.11*.

[13] SIMULIA. *Abaqus Nitinol Answer ID 1658*.

[14] J. Lubliner F. Auricchio, R. L. Taylor. Shape-memory alloys: macromodelling and numerical simulations of the superelastic behavior. *Computer Methods in Applied Mechanics and Engineering*, 146(3-4):281–312, 1997.

[15] Nitinol Development Corporation T.W. Duerig, A.R. Pelton. *Material Properties Handbook: Titanium Alloys*. ASM International, 1994.

A Abaqus

UMAT

The following is entered into the property module either in `Keywords` or in the input-file. The material name must start with `ABQ_SUPER_ELASTIC_[type of element]` for the subroutine to know which algorithm to employ.

```
*Material, name=ABQ_SUPER_ELASTIC_N3D_superelastic

*user material,consta=15
62000,0.33,62000,0.33,0.04,6.7 ,440.,540.,
11.,6.7 ,250.,220.,,0.04,,
*depvar
24,
```

MPC

This is a suggestion for a subroutine running Søvik's algorithm. It has not been tested and should be thoroughly reviewed. Note that an Intel Fortran compiler is required to run Fortran subroutines in Abaqus.

```
SUBROUTINE MPC(UE,A,JDOF,MDOF,N,JTYPE,X,U,UINIT,MAXDOF,
     * LMPC,KSTEP,KINC,TIME,NT,NF,TEMP,FIELD,LTRAN,TRAN)
C
      INCLUDE 'ABA_PARAM.INC'
C
      DIMENSION A(N),JDOF(N),X(6,N),U(MAXDOF,N),UINIT(MAXDOF,N),
     * TIME(2),TEMP(NT,N),FIELD(NF,NT,N),LTRAN(N),TRAN(3,3,N)

P = 0.4
LX0 = 10.0
LY0 = 10.0

A(1) = 1.0
A(2) = -1.0 + 2*P*(U(2,4)-U(2,3))*(LY0+U(2,3))/(LX0+U(1,2))^2
A(3) = -2*P*(U(2,4)-LY0-2*U(2,3))/(LX0+U(1,2))
A(4) = -2*P*(LY0+U(2,3))/(LX0+U(1,2))

JDOF(1) = 1
```

```
JDOF(2) = 1
JDOF(3) = 2
JDOF(4) = 2

UE = U(1,2) + 2*P*(U(2,4)-U(2,3))*(LY0+U(2,3))/(LX0+U(1,2))

RETURN
END
```